Microchimica Acta (2022) 189: 226
https://doi.org/10.1007/s00604-022-05320-7

ORIGINAL PAPER

Nanodiamond conjugated SARS-CoV-2 spike protein: electrochemical impedance immunosensing on a gold microelectrode

Santheraleka Ramanathan[1] · Subash C. B. Gopinath[1,2,3,4] · Zool Hilmi Ismail[5] · Sreeramanan Subramaniam[2,4,6]

Received: 14 December 2021 / Accepted: 25 April 2022 / Published online: 20 May 2022

Abstract

A promising immunosensing strategy in diagnosing SARS-CoV-2 is proposed using a 10-µm gap-sized gold interdigitated electrode (AuIDE) to target the surface spike protein (SP). The microelectrode surface was modified by (3-glycidyloxypropyl) trimethoxysilane to enforce the epoxy matrix, which facilitates the immobilization of the anti-SP antibody. The immunosensing performance was evaluated by integrating a nanosized (~ 10 nm) diamond-complexed SP as a target. The proposed immunoassay was quantitatively evaluated through electrochemical impedance spectroscopy (EIS) with the swept frequency from 0.1 to 1 MHz using a 100 mV_{RMS} AC voltage supply. The immunoassay performed without diamond integration showed low sensitivity, with the lowest SP concentration measured at 1 pM at a determination coefficient of $R^2 = 0.9681$. In contrast, the nanodiamond-conjugated SP on the immunosensor showed excellent sensitivity with a determination coefficient of $R^2 = 0.986$. SP detection with a nanodiamond-conjugated target on AuIDE reached the low limit of detection at 189 fM in a linear detection range from 250 to 8000 fM. The specificity of the developed immunosensor was evaluated by interacting influenza-hemagglutinin and SARS-CoV-2-nucleocapsid protein with anti-SP. In addition, the authentic interaction of SP and anti-SP was validated by enzyme-linked immunosorbent assay.

Keywords COVID-19 · Spike protein · Biosensor · Respiratory virus

Introduction

The world is currently experiencing a pandemic as a result of the newly discovered coronavirus, known as SARS-CoV-2, which has resulted in coronavirus illness 2019 [1]. Unlike pandemic caused by other coronaviruses (MERS and SARS), SARS-CoV-2 pandemic has brought a state of panic due to its rapid virus outbreak across the world, infecting ~ 200 countries and causing millions of deaths [2, 3]. Hence, the efforts in developing appropriate diagnosis, medications, and vaccination that are extremely huge to save humankind from the pandemic outbreak. The existing diagnosis technology coupled with computed tomography (CT) has been desired as a primary diagnostic strategy to recognize SARS-CoV-2 infection [4, 5]. Following that, reverse transcription-polymerase chain reaction (RT-PCR) is still upholding its stand as the highly sensitive technique to detect SARS-CoV-2 [6, 7]. Due to several drawbacks aroused, early and rapid diagnostic techniques was continued by developing loop-mediated isothermal amplification (LAMP), specific high-sensitivity enzymatic reporter unlocking (SHERLOCK), and serological detection, the invention of various strategies, yet

✉ Subash C. B. Gopinath
subash@unimap.edu.my

✉ Zool Hilmi Ismail
zool@utm.my

1 Institute of Nano Electronic Engineering, Universiti Malaysia Perlis (UniMAP), 01000 Kangar, Perlis, Malaysia

2 Faculty of Chemical Engineering Technology, Universiti Malaysia Perlis (UniMAP), 02600 Arau, Perlis, Malaysia

3 Centre of Excellence for Nanobiotechnology and Nanomedicine (CoExNano), Faculty of Applied Sciences, AIMST University, 08100 Semeling, Kedah, Malaysia

4 Centre for Chemical Biology (CCB), Universiti Sains Malaysia, 11900 Bayan Lepas, Penang, Malaysia

5 Centre for Artificial Intelligence and Robotics (CAIRO), Universiti Teknologi Malaysia, Jalan Sultan Yahya Petra, 54100 Kuala Lumpur, Malaysia

6 School of Biological Sciences, Universiti Sains Malaysia, 11800 Georgetown, Penang, Malaysia

the performances of these techniques are not in parallel with the performance exhibited by real-time RT-PCR [8]. As the pandemic spreads, an ideal detection technique for recognizing dreadful viruses is expected to be highly sensitive, user friendly, and suitable for point-of-care diagnosis, regardless of the external domains.

Carbon-based nanomaterials have a significant role in the current state of biosensor technology, particularly in medical diagnosis [9, 10]. Graphene and carbon nanotubes, which are widely used, have good electrochemical properties that contribute to a sensor's optimal performance [11]. Carbon nanodiamond has received a high interest in the last decade when it comes to bio-diagnostics. In comparison to other carbon-based materials, the sp3 carbon–comprised material has been reported as having good biocompatibility for medical diagnostics. It has also shown high fluorescence capacity, non-cytotoxicity, and cost-effective large-scale manufacturing [12, 13]. Nanodiamonds are used in fluorescent imaging, monitor bio-scaffold epithelial cells, trace the cellular regions, and regulate the immunity of a selective biomolecule. Diamonds do not require metal catalysts to be synthesized from raw materials [14]. It contributes to good cell viability and protects cells from toxicity. The polarity of diamond assists its activity in hydrophilic and hydrophobic conditions, whereas the oxides enhance its electrocatalytic activities [15]. Carbon nanodiamonds are becoming extensively common in study for amazing medical advancement progresses.

The conjugation of nanodiamonds with target prior to biosensing is least reported in literature. Like other unique nanomaterials, the diamonds are deposited in the gold electrode or integrated with other materials and inorganic compounds for achieving an enhanced sensing system. Briones and team studied the applicability of nanodiamonds on gold electrode with and without doping with inorganic polymer [16]. The nanodiamonds deposited gold electrode detected glucose and lactate based on its model enzyme and revealed a prosperous suitability for the electrochemical biosensing. Yet, the optical analysis of diamond-deposited electrode surface showed high tendency of aggregation, which increases the surface roughness and reduces the charge transduction efficiency. The author clarified that undoped diamond deposition on gold electrode sensing surface requires a polished deposition technique, which reduces the aggregation and ensure uniform distribution the nanomaterials. In the aim of reducing the diamond aggregation on gold electrode, Briones and team expanded their work by doping nanodiamonds in a sol–gel matrix of (3-mercaptopropyl)-trimethoxysilane (MPTS). The improved strategy showed good catalytic and electrochemical activity and provided the encapsulation of enzymes in the 3D diamond-sol–gel matrix [17]. As per discussed, the deposition of nanodiamonds on gold electrode in the absence of doping and modifications on electrode surface shows least performance with aggregation and insignificant for electrochemical sensing. Hence, the presented work emphasized the alternative applicability of nanodiamonds, which are integrated with target proteins, and showed remarkable performance in detecting the infectious diseases. The performed strategy eliminates doping of diamonds and complex surface modification for the aimed electrochemical biosensing. The excellent biocompatibility and non-cytotoxicity of nanodiamonds paved a potential route for its integration with biomolecules and drugs for diagnosing and treating various fatal diseases.

A futuristic electrochemical immunosensing strategy targeting SARS-CoV-2 SP using a gold interdigitated electrode (AuIDE) is proposed in this research. The sensitivity of the immunosensor was evaluated by integrating nanodiamonds with SP and compared with the immunoassay without diamond conjugation. Rigid three-dimensional tetrahedral–structured diamond nanomaterials were selected because they exhibit excellent strength and durability, as preferred for biosensing and biofunctionalization [18, 19]. The inert diamond nanomaterial exhibits a low background current and high resistance to fouling, which are extremely favorable for conjugation with protein for rapid and sensitive target detection [15]. The performance of the developed immunosensor in diagnosing SARS-CoV-2 infectious disease was determined by electrochemical impedance spectroscopy (EIS). Electrochemical quantification was determined through the redox indicator applied, followed by biomolecule interactions occurring on the sensing surface [20]. In addition, electrochemical immunoassays are cost-effective and expeditious, using low-cost equipment and materials with less expert handling involved [21, 22]. The interactions between SP and anti-SP antibody with nanomaterial integration were well defined through impedance measurements by EIS. With the relatively simple and advantages of the detection technique, the proposed strategy is recommended to be widely used in diagnosing SARS-CoV-2 infectious disease, especially for rapid and point-of-care detection to save infected people at every edge of the world.

Experimental section

Materials and reagents

A 10-μm gap-sized gold interdigitated electrode (AuIDE) with 125 electrode fingers connected by pads was purchased from Metrohm DropSens (Malaysia). His-tagged recombinant SARS-CoV-2 SP (native sequence: YP_009724390) produced in HEK293 cells was purchased from InvivoGen (China). Anti-SP antibody produced in mice was purchased from GeneTex, Inc. (North America). The recombinant SARS-CoV-2 nucleocapsid protein (NCP)

and hemagglutinin (HA) of human influenza A for specificity determination of the immunosensor were procured from GeneTex, Inc. (North America) and Sino Biological Inc. (China), respectively. Diamond nanopowder was purchased from Sigma-Aldrich (USA). Phosphate-buffered saline (PBS, 1 M, pH 7.4), potassium hydroxide (KOH), 99% ethanol, 1,1′-carbonyldiimidazole (CDI), (3-glycidyloxypropyl)trimethoxysilane (GOPTS), potassium hexacyanoferrate (III), $K_3[Fe(CN)_6]$ potassium hexacyanoferrate (II), and $K_4[Fe(CN)_6]$ were procured from Sigma-Aldrich (USA). Ethanolamine (ETA) obtained from Fisher Scientific (UK) was used as a blocking agent. Enzyme-linked immunosorbent assay (ELISA) plates and anti-mouse IgG horseradish peroxidase (HRP) were procured from Thermo Scientific (USA). ELISA coating buffer (5×) was purchased from Biolegend (Japan). 3,3′,5,5′-tetramethylbenzidine (TMB) and bovine serum albumin (BSA) were purchased from Promega (USA).

Diamond conjugation with spike protein

About 0.5 M of CDI solution was prepared using 30% ethanol. Then, 10 mg diamond nanopowder was added into 1 mL of prepared CDI solution. The mixture was mixed well using vortex and incubated for 1 h. As the reaction mixture prepared at room temperature with low mass/volume weightage, ethanol was used as the dispersant agent and additional stabilizers were eliminated [23, 24]. Based on our previous works reported, CDI linkers react with carboxyl groups of nanomaterials and resulted significant outcome in biosensing [25, 26]. The chemical surface functionalization performed on gold electrode-silicon substrate using CDI-nanomaterial composite is justified for significant target detection through various analytical methods [27, 28]. Then, the nanodiamond pellet was collected after washing the pellet twice using distilled water. The washing step was completed through centrifugation, which was performed at 10,000 × g for 5 min. A portion of the pellet was dried and characterized. The diamond morphology was determined through field emission scanning electron microscopy (FESEM, Hitachi, S-4300 SE, Japan) and field emission transmission electron microscopy (FETEM, F20-Tecnai, Columbus). Then, 1 mg washed pellet was added into 1 mL distilled water. The diamond suspension was stored at 4 °C for further analytical characterization. About 500 µL of 1 nM SP was prepared using 10 mM PBS (pH 7.4) solution to conjugate diamond with the protein molecules. The dry CDI-modified diamond (10 mg) was suspended into the prepared protein vial. The vial was incubated in room temperature for 1 h. Then, the unreactive sites on the diamond-SP were blocked using 1 M ETA. The blocked agent was added into the suspension and incubated for 15 min. Then, the diamond-protein suspension was washed using PBS buffer solution through centrifugation. Five hundred microliters of PBS solution was added to the pellet, resulting in 1 nM diamond-conjugated SP. The diamond-conjugated target protein was stored at 4 °C until further use in the immunoassay.

Immunosensor development—AuIDE

The immunosensor was chemically modified to ensure the specific detection of SP on AuIDE. The microelectrode surface was observed under optical microscopy using a 3D nanoprofiler (Hawk 3D Optical-Surface Profiler, South Korea) and a high-power microscope (HPM, Nikon Corporation, Japan). The AuIDE dimension and precision were determined using scanning electron microscopy (SEM, Jeol Ltd., Japan). The activation of the AuIDE sensing surface was initiated by dropping 20 µL of 1% KOH and incubating for 10 min. The activation generates silanol groups (SiOH) on the native oxide layer of AuIDE by instantly oxidizing and covalently form bonding with hydroxyl (OH-). The activation of sensor with KOH is considered a "click" reaction, which ensures the supramolecular covalent interaction and subsequent covalent fixation. Based on our previous studies, the strong basal architecture with relatively simple activation strategy is mandatory to trigger the sensing surface functional groups for further functionalization, which is evaluated through the EIS impedance recording [27, 29, 30]. Then, 20 µL of 2% GOPTS solution was drop-cast on AuIDE to create an epoxy matrix, which is highly reactive with amine and carboxyl bases. The sensing surface was washed by dropping 20 µL of 10 mM PBS solution after a 1-h incubation with the linking agent [26, 31]. As the bioprobe for SP detection, 20 µL of 1 µM anti-SP antibody was immobilized on AuIDE and incubated for 1 h. The unbound antibodies were removed by washing with 20 µL of PBS solution. Moreover, the unreactive active regions of AuIDE were blocked with 20 µL of 1 M ETA solution. SP, as the target of the assay, was prepared in the femtomolar to nanomolar range of concentrations (1 fM to 1 nM) from 100 nM stock. A 20 µL aliquot of 1 fM SP was immobilized on the sensing surface and incubated for 5 min. Then, the surface was washed with 20 µL of PBS solution to remove the unbound target. The detection of SP on AuIDE was evaluated through electrochemical impedance spectroscopy (EIS) using a Novocontrol alpha high-frequency analyzer (Novocontrol Technologies GmbH, Germany). The working and reference electrodes of the AuIDE were fixed with the EIS probes for impedance measurements. Redox solutions consisting of 10 mM PBS and 5 mM $[Fe(CN)6]^{3-}$ and $[Fe(CN)6]^{4-}$ were used to characterize the Faradaic measurement with EIS analysis. AuIDE A 20 µL of redox solution was dropped on the sensing surface and the EIS measurement was started to record. The EIS measurements were recorded with the swept frequency from 0.1 to 1 MHz using

a 100 mV_{RMS} AC voltage supply. Another type of immunoassay was performed using diamond conjugated SP as the target to evaluate the efficiency of diamond-conjugated SP in detecting SARS-CoV-2 infectious disease on the anti-SP antibody-modified AuIDE. The impedance spectra for the analyses were plotted for the real, Z′ and imaginary parts, Z″ of impedance. The AuIDE was fixed in the two-electrode probe station of EIS, throughout the experiment performed to ensure uniform charge distribution over the electrode surface. A 20 µL of analyte volume was fixed to be used in the overall experiment. A conservative washing step using 10 mM PBS solution was performed in the interval of each surface modification and in the interval of detecting target protein from the lowest to the highest concentration. The analytical performance of the sensor was validated through the mean impedance and standard deviation of detection readings using three electrode surfaces ($n = 3$), which also emphasized the repeatability and accuracy of electrochemical impedance measurements. Figure S1 illustrates the steps of AuIDE electrode surface preparation and nanodiamond conjugation with SP for the impedimetric immunosensing of SARS-CoV-2.

Enzyme linked immunosorbent assay (ELISA)

The specific binding of recombinant soluble SP with anti-SP antibody was validated through ELISA. SP at concentrations ranging from 1 pM to 100 nM was prepared using 1 × coating buffer. Then, 50 µL of target was coated into the "ELISA plate" wells and incubated at 4 °C overnight. Consecutive washings at each step were performed using 300 µL of PBS-Tween 20 solution. Then, the wells were blocked using 300 µL of 2% BSA solution. The anti-SP antibody was diluted 1:1000 from the stock. Approximately 50 µL of diluted primary mouse antibody was coated in the wells and allowed to interact with the coated target for 1 h. Next, anti-mouse antibody–conjugated HRP at 1:1000 was coated and incubated for 1 h to allow the interaction between primary and secondary antibodies. Finally, TMB substrate respective to HRP enzyme was added to the wells. The color change in the wells was observed closely, and the interaction of SP and anti-SP antibody was determined by recording the absorbance reading using a UV-Nanodrop (DS-11/DS-11, Denovix, USA).

Results and discussion

An ideal biosensor for rapid detection of SARS-CoV-2 disease is expected to have excellent portability, sensitivity, and precision. Excellence in detecting and discriminating various sample detection limits is preferred to diagnose fatal disease at the early stage of virus infection. In this approach, an interactive analysis was performed on AuIDE to evaluate the detection of SARS-CoV-2 using soluble recombinant SP and its anti-SP antibody. IDE sensors have been reported for their efficiency in recognizing specific interactions with varying biomarkers. To improve the detection sensitivity, nanodiamond-conjugated SP was integrated into the developed immunosensor. EIS measurements provide detailed information on the diamond and biomolecule interactions that take place on the immunosensor and aid in determining SP. Figure 1 shows a schematic illustration of the proposed strategy in detecting SARS-CoV-2 SP by an anti-SP antibody on AuIDE integrated with nanodiamond-conjugated SP.

AuIDE morphology — high resolution surface imaging

Morphological examination revealed the precision of the AuIDE sensing surface. Figure 2a shows the digital image of AuIDE used. Optical images of AuIDE electrodes and junctions were observed under HPM (Fig. 2b–2c). The dimensions of the sensing surface were verified through SEM imaging (Fig. 2d), which revealed that the gap and electrode dimensions differed by ~ 0.4 µm from the designed dimensions. The electron microscopic image of the electrode junction indicates the active surface of AuIDE without any foreign substances (Fig. 2e). The smoothness of AuIDE between its gold electrode and silicon substrate was visualized through a 3D profiler (Fig. 2f–2g). Moreover, the roughness profile indicates that the height of the electrode and gap on AuIDE is exact (Fig. 2h), which further affirmed the indistinguishable color of the electrode and gaps indicated through 3D images. The average height of AuIDE used is ~ 48.9 µm.

Nanodiamond morphology — size and shape observations

The commercially purchased nanodiamond was modified with CDI linker to activate its functional groups for covalent protein conjugation. The size and shape of the nanodiamonds were determined through FETEM and FESEM analyses. Figure 2i–2k shows the electron microscopic image of diamond under FETEM at various scales, revealing the uniform size of modified diamonds. The distribution was uniform and compact, as no space between the diamonds was observed in the electron microscopic images. Figure 2l shows an enlarged electron microscopic image of nanodiamond with the size measured using the FETEM microscopic tool. Figure 2m–2n shows the uniform spherical shape of nanodiamonds, observed through FESEM imaging. Based on the electron microscopic morphology, the average size of diamond nanoparticles is ~ 10 nm, observed at their spherical shape. The elemental composition of diamond was identified through energy dispersive spectroscopy (EDS).

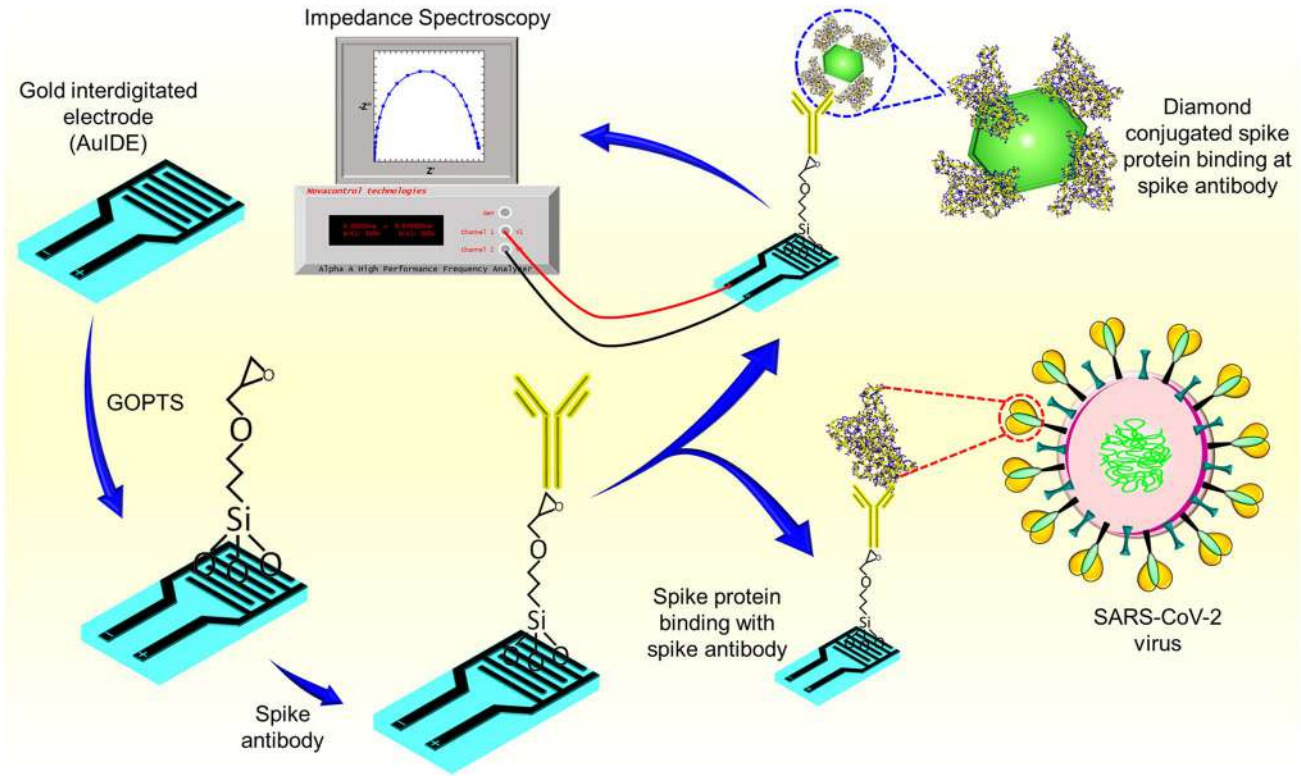

Fig. 1 Schematic illustration of SP detection. Anti-SP was used on a gold microelectrode as a prognostic approach in diagnosing life-threatening SARS-CoV-2. Impedance measurements of AuIDE in the presence of SP integration with and without nanodiamonds were evaluated by electrochemical spectroscopy

The EDS spectra shown in Fig. 2o emphasized that the diamond consisted of 94.58% carbon and 2.32% and 2.75% oxygen and nitrogen, respectively. The platinum (Pt) that appeared in the EDS spectra was due to Pt used for FESEM coating for electron microscopic analysis.

Surface chemistry analysis — functionalization

The stability of AuIDE used in the development of the immunosensor was validated through reproducible EIS measurements (Fig. 3a). The Nyquist plot attained by testing three bare AuIDEs indicates the R_s and R_{ct} of the microelectrodes. The kick-off R_s value for the three bare AuIDEs is the same [Fig. 3a (i)], which demonstrates the accuracy in reproducibility of the devices. The variation observed with the Z′ of the three bare devices may arouse due to the contaminants existing on the sensing plate. The storage condition and sensing surface exposure to air molecules may induce oxidation on the glass silicon substrate, which may increase or reduce the bare impedance readings [22]. Bare AuIDE 1 showed high Z′ value compared to bare AuIDE 2 and 3, which may depict that the degree of oxidation on AuIDE 1 is less than the other electrode surfaces. It is compulsory to store the microelectrodes in dry cabinet to avoid contaminant accumulation on sensing surface. Referring on the handling of microelectrodes at micro-scaled gap sizes, the possibilities of nano-scaled materials or contaminant to be existed on the bare electrode surface is significantly high. The mean Z′ value at 2 Hz against the analyte added in the step of surface chemistry on immunosensor development is shown in Fig. 3b. Modification of AuIDE with GOPTS created a moderate resistive layer with ~ 48 kΩ real-part impedance. Following that, the immobilization of anti-SP generated a high Z′ at ~ 88 kΩ, indicating the highly insulating characteristics of the antibody and its high electron-transfer rate in the presence of its active sites. The blocking of AuIDE with ETA reduces the charge resistance. The reduction in the R_{ct} value may result from the formation of positively charged anion cloud due to the complexes formed with the epoxy matrix of GOPTS and the blocking agent, ETA [32, 33]. The target detection was compared using ETA as the baseline to evaluate the sensor analytical performances. Figure S2 indicates the impedance spectra and mean Z′ evaluated upon the surface functionalization and the details on selecting ETA as the baseline for the impedimetric analysis. The addition of a target on antibody-immobilized AuIDE gives a higher Z′ (44 kΩ) than ETA (24 kΩ), indicating the specific binding of SP and anti-SP and thus justifying the precision of surface chemistry in detecting SP.

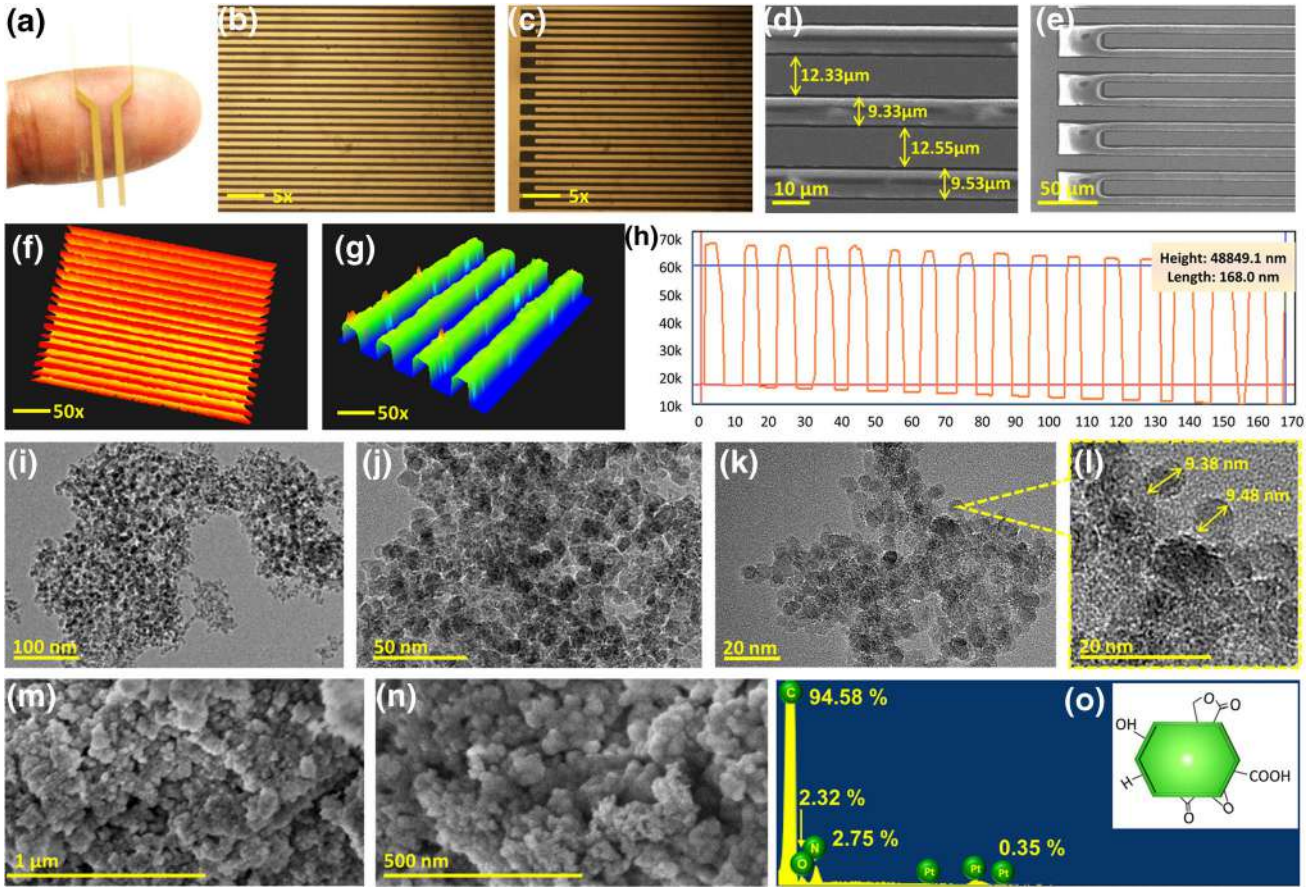

Fig. 2 Morphological analysis of AuIDE and nanodiamond. **a** Digital image of AuIDE. HPM images of AuIDE **b** electrode fingers and **c** electrode junctions. **d** Electron microscopic image under SEM. Shows the dimensions of electrode and gaps measured. **e** Sharp edges of electrode junction with AuIDE. **f–g** 3D optical images of AuIDE. The height difference between the electrode and gap on the sensing plate was visualized. **h** Roughness profile of AuIDE analyzed under a 3D profiler. **i–l** FETEM images of nanodiamonds. Uniform nanosized particles were revealed at various scales. **m–n** Spherical shape of diamond observed from the FESEM images. **o** EDS analysis of diamond from FESEM. Diamond structure is inserted in the plot

Spike protein-antibody interaction on AuIDE

The impedance spectra obtained when the anti-SP antibody immobilized AuIDE were evaluated with SP from 1 fM to 1 nM (Fig. 4a). The Nyquist plot obtained from EIS measurements of AuIDE represents the Randles circuit, which expresses the redox solution resistance (R_s), charge transfer resistance (R_{ct}), and double layer capacitance (C_{dl}) [22, 34]. The R_s value is expected to be similar for every EIS reading, as the volume of redox solution (20 µL) used is the same for

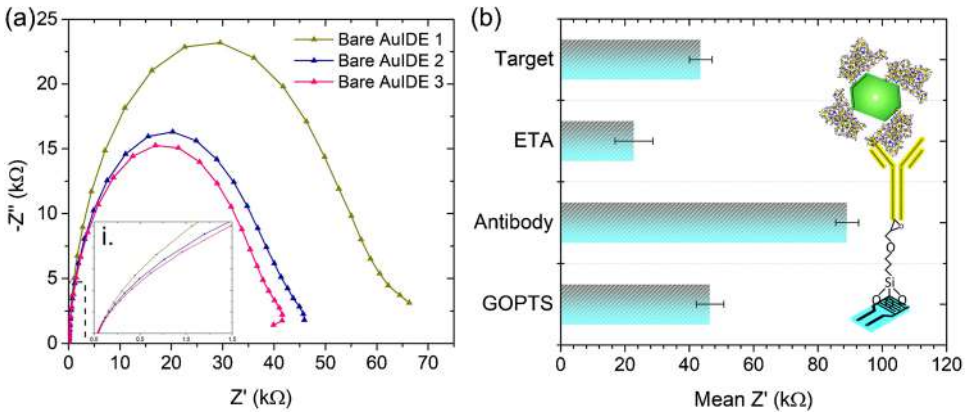

Fig. 3 **a** Reproducibility assessment conducted with three bare AuIDEs. Electrochemical characterization of SP and anti-SP on AuIDE. **b** Mean Z′ against the steps of surface chemistry performed on the AuIDE

every measurement. The increment in the R_{ct} value represents the weight of charge transfer upon interaction between the developed immunosensor and different concentrations of SP. The impedance spectra were discussed based on the changes observed in the real part impedance, Z', which indicates the charge transfer resistance from the redox solution to the base of the immunosensor. The Nyquist spectra generated with 1 and 10 fM SP were lower than those generated with ETA. The intensity of charge transfer was insignificant with the concentration, indicating insignificance in detecting the interaction between the anti-SP antibody and protein. From 100 fM to 1 nM, a notable increase was observed in the Nyquist plot, revealing that SP and anti-SP antibody interactions occurred. A huge gap was noticed between Z′ of 1 to 10 pM SP and then to 100 pM SP. The gap between the Nyquist plots indicates that the detection range of SP on the developed immunosensor falls in the picomolar range of concentration. Thus, the detection of SP on anti-SP immobilized AuIDE was performed in the narrowed range of target concentrations. Figure 4b shows the impedance spectra plotted by analyzing SP from 1 to 64 pM. A linear accretion in Z′ was observed from 1 to 8 pM. Z′ increases by ~ 1.5-fold from 1 to 8 pM at each interval target. The Z′ difference between 8 and 16 pM was small. In addition, the Nyquist spectra of 32 and 64 pM SP went downward against the linear direction. This indicates that the saturation point for SP interaction with 1 µM anti-SP

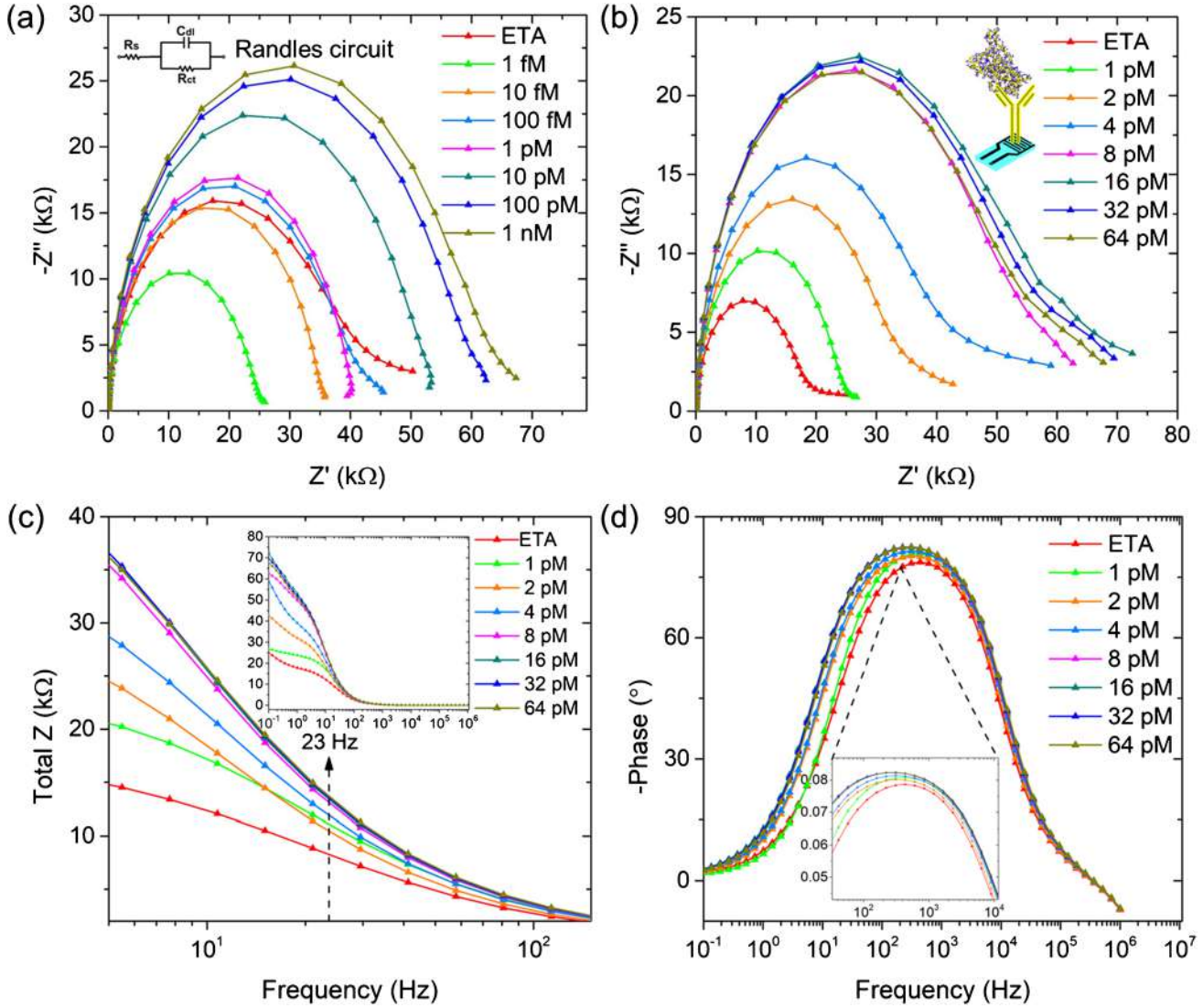

Fig. 4 **a** Impedance spectra of AuIDE immobilized with anti-SP interaction. SP concentrations from 1 fM to 1 nM were used. **b** Impedance spectra with narrowed SP concentration. The target concentration constricted at a detection range of 1 pM to 64 pM indicates the lowest detection of SP on bioprobe-attached AuIDE at 1 pM. **c** Response of total impedance against the frequency. The represented Bode plot reveals the equilibrium response of SP detection observed at 23 Hz. The Fig. inset shows the overall impedance response against swept frequency from 0.1–1 MHz. **d** Phase angle versus the frequency plot of SP detection on AuIDE

immobilized AuIDE was at 8 pM SP. The linear detection of SP at the lower picomolar range emphasizes the success of immunosensors developed for detecting SP for diagnosing SARS-CoV-2 infectious disease.

Figure 4c shows the Bode plot generated with the total "Z" values against the frequency supplied (0.1 to 1 MHz) for SP and anti-SP interaction on the developed immunosensor. The Bode plot shows that the total "Z" values increase from 1 to 16 pM SP, resembling the similar trend observed in impedance spectra (Fig. 4b). A significant variation in the total "Z" was observed at 23 Hz before it reached a stagnant state at 10^2 Hz up to 10^6 Hz. Figure 4d shows the phase angle revealed by the immunosensor with immobilized SP. In good agreement with the total "Z" (Fig. 4c), the phase angle spectra show a significant change at ~ 23 Hz. The active frequency and its real part impedances for different concentrations of SP were evaluated to determine the sensitivity performances.

Diamond-conjugated spike protein-antibody interaction on AuIDE

The electrochemical measurements of anti-SP antibody–immobilized AuIDE were recorded by analysis with diamond-conjugated SP from 0.25 to 8 pM. The concentration range selected for evaluation was reduced from the previous immunoassay (1–64 pM), as the conjugation of nanodiamonds is expected to improve the detection strength of SP on the sensing plate. Figure 5a shows the impedance spectra obtained from the diamond-conjugated SP interaction on the developed immunosensor. It was proven that the performance of the immunosensor was excellent when diamond-conjugated SP was used as the target. Linear detection of SP was apparent from the 0.5 to 8 pM diamond-conjugated protein. The Z′ impedance value was immensely reduced from 25 kΩ (Fig. 4b) to 4 kΩ (Fig. 5a) when a 1 pM target concentration interacted with the immunosensor. The reduction in Z′ denotes the highly moving electron with the target interaction and conjugation of diamond on the sensing plate. This further enhances the electrical conductivity of the sensor, ~ 6250-fold better than the interaction exhibited without diamond. ETA exhibited 3 kΩ of Z′, and the value was increased to 4 kΩ at 1 pM. The small increase in the Z′ value indicates that diamond-conjugated SP is detected on chemically modified AuIDE. As the diamond-conjugated protein concentration was increased from 1 to 2 pM, the increase in Z′ was ~ 1.6-fold higher, which indicates the significant

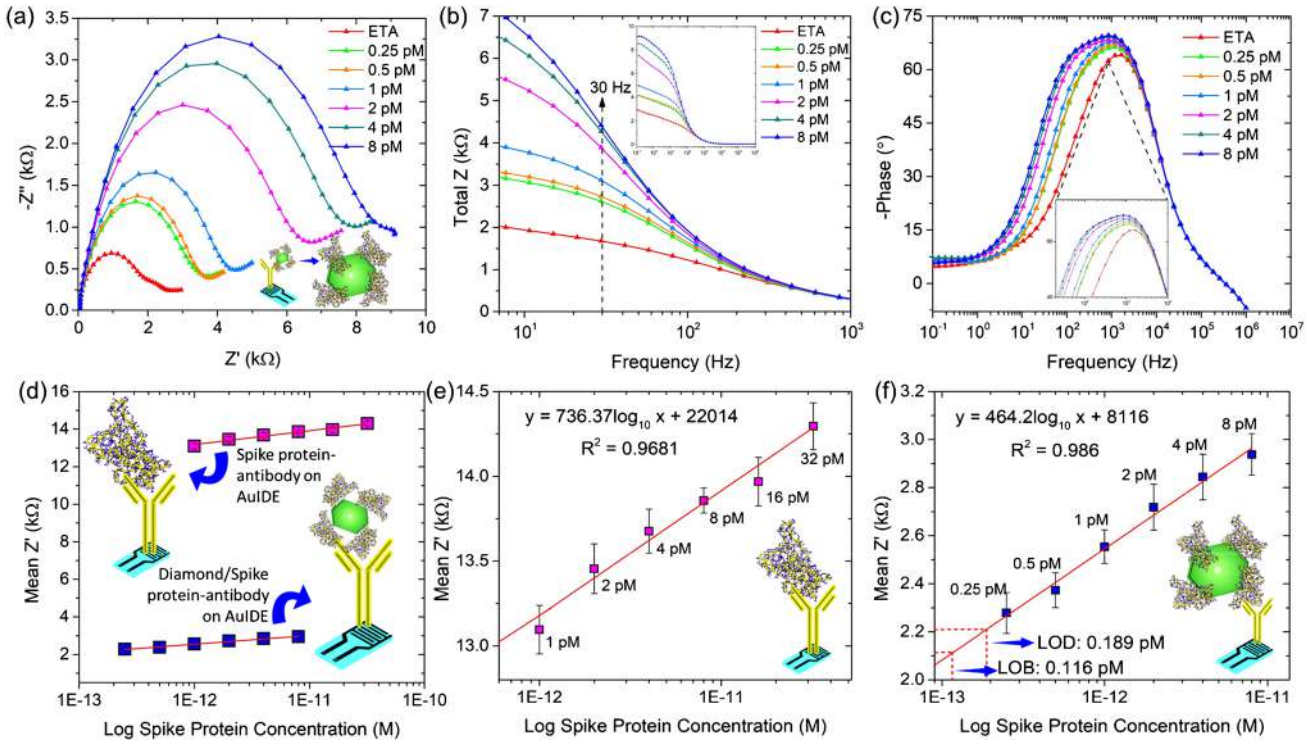

Fig. 5 Analytical performances of nanodiamond-incorporated AuIDE for detecting NCP. **a** Nyquist plot shows the detection of diamond-conjugated SP with anti-SP immobilized on AuIDE. **b** Bode plot constructed with the total impedance against frequency. The active range of SP detection occurs at 30 Hz. **c** Phase angle versus frequency of the immunosensing system. **d** Linear calibration lines of immunoassay performed with and without nanodiamond integration. **e** Calibration plot for SP and anti-SP interaction. The detection ranging from 1 to 32 pM shows a determination coefficient of $R^2 = 0.9681$. **f** Calibration plot of AuIDE immunosensing with diamond-conjugated SP. The linear detection ranges from 0.25 to 8 pM with $R^2 = 0.986$ shows a limit of detection equal to 0.189 pM

interaction of anti-SP antibody on AuIDE. Following that, a linear detection trend was observed from 2 pM (7.8 kΩ) to 8 pM (9.2 kΩ), emphasizing the significance of diamond in enhancing the sensitivity and linearity in detecting the target protein on the developed immunosensor. The linear accretion in Z′ explains the increase in the rate of charge transfer aroused with countless SP and anti-SP interactions on AuIDE. The decrease in the Z′ with diamond conjugated SP as the target than the SP alone is mainly contributed by the physiochemical of diamond nanomaterial. Conjugation of diamond with biomolecules enables high density SP protein immobilization due to its excellence in high surface area/volume and its enhancement in generating feasible spatial arrangement for the sensing mechanism. Moreover, diamond resists fouling and upholds good biocompatibility with protein, which improves the sensitivity and performance of the immunosensor [35, 36]. The ability of oxide groups in carbon nanodiamond excel its electrocatalysis and electrical conductivity. The favorable polarity groups of the diamond surface region provide an excellent platform in controlling the biomolecule adhesion and enhancing the bioconjugation of SP on the sensor region. As the biomolecules adhere to the electrode surface, the polarity of nanodiamonds exhibits strong antifouling characteristics with its unique electrostatic and hydrophilic interactions. Due to the good biocompatibility, carbon nanodiamond ensures high antifouling resistance and establish a good electrocatalytic activity. With its unique electrostatic and hydrophilic interactions, diamond nanomaterial improves the sensitivity and performance of the immunosensor [37]. Figure 5b and 5c show the total Z and phase angle against the swept frequency, respectively. The plots indicated that a high rate of charge transfer occurred in the low frequency range (0.1–100 Hz). The active frequency in detecting SP using the developed immunosensor was determined at 30 Hz based on the active frequency range in the Bode plot and the maximum phase angle of the system. The frequency response fits a system based on the parameters and materials utilized. The electrolyte of a system defines the physics of intermolecular change upon detection and stimulate the impedance response. The conjugation of diamond with target protein alters the surface capacitance, which is reflected in the change of frequency domain in overall. Therefore, the active frequency selected for an individual sensing mechanism varies with the change of parameters involved in the system [38–40].

Immunosensor sensitivity: comparative analysis

The sensitivity of the developed immunosensor was evaluated with SP and diamond-conjugated SP as targets for detecting SARS-CoV-2. Figure 5d shows a linear calibration curve generated by the linear detection measurements using SP and diamond-conjugated SP on the immunosensor. It reveals that anti-SP immobilized AuIDE has a lower Z′ in the low frequency range using diamond-conjugated SP as the target compared to the immunoassay performed without diamond. Moreover, the linear regression lines plotted by comparing immunoassay with and without diamond incorporation indicate the performance of diamond-based immunoassay in detecting the target at lower concentration range and hence emphasize the highly sensitive immunoassay. Figure 5e shows the calibration curve plotted with the mean Z′ values obtained at 23 Hz versus the logarithm of SP concentrations. The linear calibration curve ($n=3$) represents the linearity in detecting SP targets from 1 to 32 pM. A linear equation obtained from the calibration curve was $y=736.37\log10\times+22{,}014$. The coefficient determination attained with the linear calibration was $R^2=0.9681$. In comparison, Fig. 5f shows the calibration curve attained by EIS measurements of the immunosensor using diamond-conjugated SP. The linear equation attained from the analysis was $y=464.2\log10\times+8116$. The determination coefficient obtained was $R^2=0.986$. This emphasizes that the diamond-conjugated SP interaction on anti-SP immobilized AuIDE has shown good sensitivity and linearity in detecting SP in the low picomolar range. Nonetheless, SP without diamond conjugation exhibited low precision and accuracy, which revealed by the low R^2 value attained [41, 42]. Diamond-conjugated SP showed remarkable linear detection with a higher R^2, indicating the high sensitivity and performance of the developed immunosensor. A linear equation was evaluated for computing the limit of blank (LOB) and the limit of detection (LOD) based on the quantification reported [43], shown as:

$$\text{LoB} = \text{mean blank} + 1.645\ (\text{SD blank})$$
$$\text{LoD} = \text{LoB} + 1.645\ (\text{SD low concentration sample})$$

Based on the computational evaluation, the LOD of the developed immunosensor with diamond-conjugated SP is 189 fM for approximately 116 fM LOB. The values obtained through the linear regression plot and LOD calculations justified the high-performance immunoassay incorporating nanodiamonds for targeting the SARS-CoV-2 SP on a gold microelectrode. The immunoassay denoted a promising immunoassay strategy with 10 min of reaction time for probe-target interaction. Immediate EIS readings are an added advantage for the prompt evaluation of immunosensor analytical performance. The propitiousness of nanodiamonds is perceptible to addressing the high sensitivity of immunoassays, where the LOD reaches the femto level of SP detection, without additional modification of the nanodiamond chemistry and microelectrode sensing functionalization. The LODs attained in the present research were compared with those in recent work on detecting SARS-CoV-2 SP (Table 1). The optimization of nanodiamond weight/volume ratio and the

chemical linking of diamond-SP target serve as the limitation of the work, which will be studied in our future studies to attain low analyte and high-performance detection assay. The developed immunosensor using AuIDE is reusable prior to the detachment of chemical and biomolecules modification on the sensing surface by the strategic washing with Piranha solution. Piranha solution was prepared in 3:1 ratio of sulfuric acid and hydrogen peroxide under chemical hood to clean the electrode surface, which has been coated with KOH, GOPTS, and anti-SP antibody. AuIDE carefully immersed into the Piranha solution for one minute and thoroughly washed with distilled water. The air-dried AuIDEs are reusable for another cycle of immunoassay. The 1-min immersion in strong Piranha solution is significant for washing the electrode surface without disrupting the electrode bonding pads and regenerate the interdigitated electrode [44]. The potential of AuIDE for its extended storage lifetime for several months is significant, prior to its proper desiccated package and storage condition. Upon modification of the sensing surface with chemical and biomolecule agents, the surface activity may reduce by 25% after 3 weeks and may result in sensor failure without proper storage and handlings.

Immunosensor selectivity and specificity analysis — spiking in human serum

The prospect of the developed immunosensor for clinical SP detection was determined using diamond-conjugated SP (1 fM to 100 pM) spiked in human serum. Figure 6a shows the Nyquist plot generated with different serum concentrations to determine the optimized serum dilution for SP spiking. Based on the plot, a 1:100 dilution of serum was chosen for spiking with targets, as it shows a negative trend (high value) in Z′ with the stock serum. The figure inset in Fig. 6a shows the average impedance obtained at three subsequent washings performed on AuIDE using different serum concentrations to indicate the least variation in the subsequent rinse cycles of the dilution buffers and hence affirm the least effect of serum dilutions on the Nyquist plot [45, 46]. The impedance spectra shown in Fig. 6b indicate the detection of diamond-conjugated SP spiked in human serum on AuIDE. A prominent detection range was observed at 0.25–1 pM of diamond-conjugated protein. The Z′ value attained by 250 fM human serum-diluted diamond-conjugated SP (12 kΩ) was threefold higher than the target diluted in PBS (4 kΩ). The significant elevation in the Z′ value indicates the large noise in the electrolyte system due to the presence of multiple types of biomacromolecules in human serum. However, the linear detection Nyquist plot observed in Fig. 6b represents the excellent performance of the developed immunosensor using AuIDE in detecting diamond-conjugated SP in human serum. The detection of SP spiked in human serum consists of large and intensive macromolecules such as globulin (~66 kDa) and albumin (~150 kDa) [47]. The detection of diamond-conjugated SP diluted in human serum at lower pico-molar range evidences the potentiality of the immunosensor for specific and selective SP detection in the high molecular weighted proteins system and its interferences [48, 49]. This emphasizes the potential of the developed immunosensor with diamond integration for clinical applications of infectious disease diagnosis. The carbon nanodiamond vital surface functional groups and its electrocatalytic activity on the developed immunosensor eliminate the biofouling as it upholds high antifouling resistance. As the biomolecules adhere to the electrode surface, the polarity of nanodiamonds exhibit strong antifouling characteristics with its unique electrostatic and hydrophilic interactions [50, 51]. In an approach of real-time POC diagnostics of SARS-CoV-2, the developed immunosensor with carbon nanodiamond conjugated SP as the target is expected to be satisfyingly sensitive to capture the SP target among the interference proteins in serum on the anti-SP immobilized AuIDE. The specificity of the immunosensor developed for detecting SP was examined using HA and NCP as negative proteins. Figure 6c shows the mean Z′ values revealed by the immunosensor when tested with negative proteins, followed by positive diamond-conjugated SP. The results denote that HA and NCP protein give nonspecific binding, as shown in the schematic diagram inserted in

Table 1 Recent reports on SARS-CoV-2 diagnosis using SP as the targeted antigen

Detecting strategy	Electrode material	Nanomaterial	Detection range	LOD	Reference
Microfluidic assay	Glass substrate	Gold nanospikes	0.1–10 ng/mL	0.08 ng/mL	[7]
Lateral flow immunoassay	Screen printed electrodes	Conducting polymer	0–200 ng/mL	1.86×10^{5} copies/mL	[52]
Electrochemical immunoassay	Screen printed electrodes	Graphene sheets	100 fg/ml to 100 pg/mL	1.6×10^{1} pfu/mL	[53]
Electrochemical immunoassay	Screen printed electrode	Nil	1 pg/mL to 10 ng/mL	1 pg/mL	[54]
Electrochemical immunoassay	Indium tin oxide electrode	Gold nanoparticles	0.002–100 pg/mL	0.577 fg/mL	[55]
Electrochemical immunoassay	Gold	Carbon nanodiamond	1–8 pM	0.189 fM	Current work

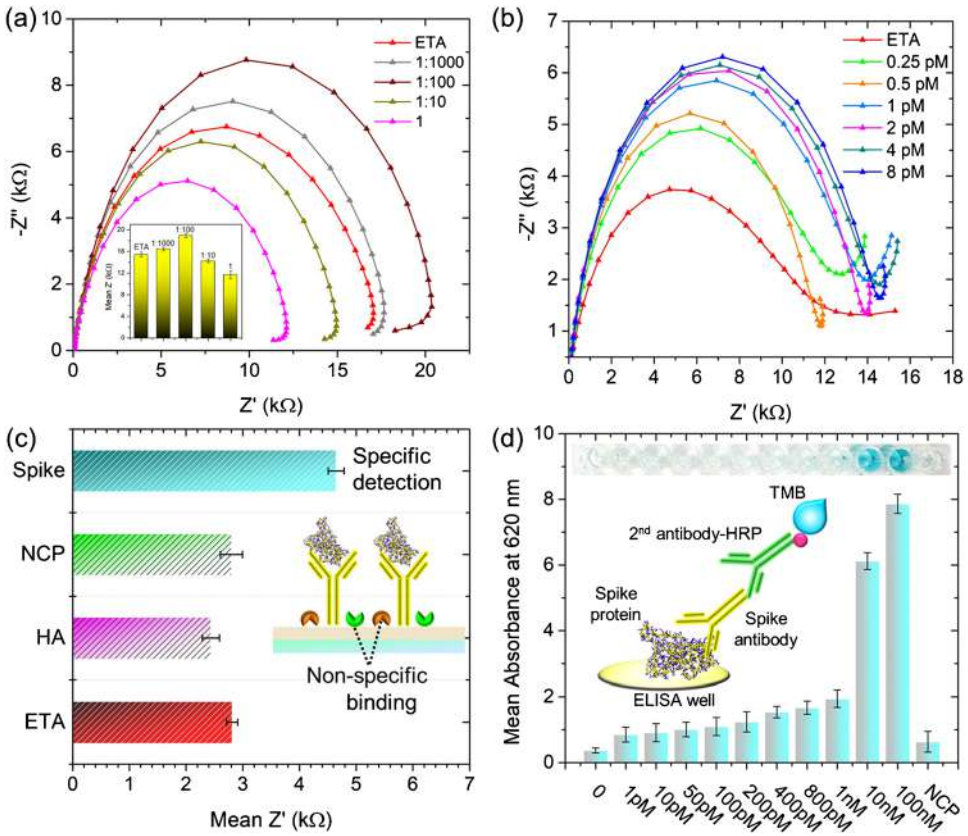

Fig. 6 Selectivity and specificity assessments. **a** Impedance response of human serum and its dilution on anti-SP immobilized AuIDE. The inserted figure shows the average impedance obtained at three subsequent washings performed using serum dilutions. **b** Detection of diamond-conjugated SP diluted in serum on the developed immunosensor. **c** Cross-specificity analyses of anti-SP immobilized AuIDE. The mean Z′ value of HA and NCP indicates the nonspecific detection of negative proteins. **d** Validation of SP and anti-SP interaction. The absorbance readings and inserted digital images of the ELISA justified the SP interactions

Fig. 6c, whereas diamond-conjugated SP gives specific detection. The results justify the ideal condition of the developed immunosensor in recognizing single and complementary target antigens. This condition is attained by the ideal functionalization of the anti-SP antibody on a gold microelectrode, which is able to capture SP in the presence of multiple macro- and micro-molecules found in serum. In addition, the carbon nanodiamond integrated with SP enhances the high-speed and high-density antibody-antigen specific binding with its advantageous large surface area and its resistance to biofouling, especially in the presence of other molecules. Hence, the results emphasized the significant selection and sensitive detection of SARS-CoV-2 SP in serum and denote a promising strategy for implementation in clinical trials.

Immunosensor and spike protein binding: validation

The binding between recombinant SP and anti-SP was validated through ELISA as a preliminary SP detection assay before biosensor applications. Figure 6d shows the absorbance readings recorded at 620 nm with tested SP targets in the range of 1 pM to 100 nM concentrations. A gradual increase in the absorbance measurement was notable from 1 pM to 1 nM SP, validating the specific binding of recombinant SP and its antibody procured for this research. Maximum absorbance numbers were recorded at 10 nM and 100 nM SP, which were ~ threefold higher than 1 nM SP, indicating innumerable protein-antibody binding of the SARS-CoV-2. This result is in good agreement with the dark blue color that appeared in the ELISA well (Fig. 6d; inset), corresponding to the high amount of SP immobilized. In addition, the specificity of SP protein-antibody binding was evaluated by immobilizing 1 nM NCP target in the ELISA well. The negligible absorbance and its corresponding clear ELISA well evidenced the specific detection of SP using procured protein and antibody for recognizing SARS-CoV-2 infectious disease. It has been estimated that infected person carries 10^9–10^{11} virions with the highest infection, at a total mass of 1–100 µg. Furthermore, accounting 30–40 spike trimers on each SARS-CoV-2 virion, it was calculated that the ratio of neutralizing antibodies to viral spike proteins is 10^3–10^5 (neutralizing antibodies per spike protein) [56]. With this calculation, the current sensor behaves better with several fold higher sensitivity.

Conclusion

The global threat caused by the SARS-CoV-2 infectious disease urges the development of rapid, sensitive, and selective diagnostics in controlling and alleviating the pandemic

consequences. The presented research proposed a prognosticative electrochemical immunoassay strategy using AuIDE in detecting SP by anti-SP antibody as a promising strategy for diagnosing SARS-CoV-2 virus. The electrochemical immunoassays were evaluated with and without nanodiamond conjugation to SP. It is apparent that the diamond-conjugated SP showed a superior linear detection trend in the lower picomolar range of concentration in comparison to the immunoassay performed without integration of diamond nanomaterial. The developed immunoassay worked well with diamond-conjugated SP spiked in human serum, which justifies the satisfactory performance of the proposed strategy in terms of selective and stable detection. The presented work emphasizes the potential route of nanodiamond conjugation with targets of infectious diseases for enhanced electrochemical detection without complex modification on electrode surface. The gold electrode surface modification using low molecular weighted chemical linker shows an inexpensive and straightforward surface modification for biomolecule immobilization. Nevertheless, the sensitivity of the immunoassay was attained at low detection limit with the unique role of diamond integrated with target protein. The strategy is recommended in boosting the performance of immunosensing strategies for rapid identification and quantification of SARS-CoV-2 virus infection. Furthermore, it is applicable to other sensors considering the method of surface functionalization. However, a drawback in the proposed sensing system is the optimization for the carbon nanodiamond, as the physiochemical property of diamond elevates the surface kinetic on the probe conjugated AuIDE.

Supplementary Information The online version contains supplementary material available at https://doi.org/10.1007/s00604-022-05320-7.

Funding This work was financially supported by grant (R.K130000.7343.4B617) under ASEAN University Network Southeast Asia Engineering Education Development Network (AUN/SeedNet) Special Program for Research against COVID-19 (SPRAC) and a grant (9001-00596) from Universiti Malaysia Perlis.

Declarations

Competing Interests The authors declare no competing interests.

References

1. Zhao H, Liu F, Xie W et al (2021) Ultrasensitive supersandwich-type electrochemical sensor for SARS-CoV-2 from the infected COVID-19 patients using a smartphone. Sensors Actuators, B Chem 327:128899. https://doi.org/10.1016/j.snb.2020.128899
2. Taleghani N, Taghipour F (2021) Diagnosis of COVID-19 for controlling the pandemic: a review of the state-of-the-art. Biosens Bioelectron 174:112830. https://doi.org/10.1016/j.bios.2020.112830
3. Lee JH, Choi M, Jung Y et al (2021) A novel rapid detection for SARS-CoV-2 spike 1 antigens using human angiotensin converting enzyme 2 (ACE2). Biosens Bioelectron 171:112715. https://doi.org/10.1016/j.bios.2020.112715
4. Huang Y, Yang C, Xu XF et al (2020) Structural and functional properties of SARS-CoV-2 spike protein: potential antivirus drug development for COVID-19. Acta Pharmacol Sin 41:1141–1149. https://doi.org/10.1038/s41401-020-0485-4
5. Khan MZH, Hasan MR, Hossain SI et al (2020) Ultrasensitive detection of pathogenic viruses with electrochemical biosensor: state of the art. Biosens Bioelectron 166:112431. https://doi.org/10.1016/j.bios.2020.112431
6. Cady NC, Tokranova N, Minor A et al (2021) Multiplexed detection and quantification of human antibody response to COVID-19 infection using a plasmon enhanced biosensor platform. Biosens Bioelectron 171:112679. https://doi.org/10.1016/j.bios.2020.112679
7. Funari R, Chu KY, Shen AQ (2020) Detection of antibodies against SARS-CoV-2 spike protein by gold nanospikes in an optomicrofluidic chip. Biosens Bioelectron 169:112578. https://doi.org/10.1016/j.bios.2020.112578
8. Zhang M, Li X, Pan J et al (2021) Ultrasensitive detection of SARS-CoV-2 spike protein in untreated saliva using SERS-based biosensor. Biosens Bioelectron 190:113421. https://doi.org/10.1016/j.bios.2021.113421
9. Ramanathan S, Gopinath SCB, Md. Arshad MK, Poopalan P, (2019) Multidimensional (0D–3D) nanostructures for lung cancer biomarker analysis: comprehensive assessment on current diagnostics. Biosens Bioelectron 141:111434. https://doi.org/10.1016/j.bios.2019.111434
10. Ramanathan S, Poopalan P, Gopinath SCB et al (2021) Surface charge transduction enhancement on nano-silica and - alumina integrated planar electrode for hybrid DNA determination. Mater Chem Phys 265:1–11. https://doi.org/10.1016/j.matchemphys.2021.124486
11. Ginés L, Mandal S, Morgan DJ et al (2018) Production of metal-free diamond nanoparticles. ACS Omega 3:16099–16104. https://doi.org/10.1021/acsomega.8b02067
12. Basso L, Cazzanelli M, Orlandi M, Miotello A (2020) Nanodiamonds: synthesis and application in sensing, catalysis, and the possible connection with some processes occurring in space. Appl Sci 10:1–28. https://doi.org/10.3390/APP10124094
13. Mochalin VN, Shenderova O, Ho D, Gogotsi Y (2012) The properties and applications of nanodiamonds. Nat Nanotechnol 7:11–23. https://doi.org/10.1038/nnano.2011.209
14. Chauhan S, Jain N, Nagaich U (2020) Nanodiamonds with powerful ability for drug delivery and biomedical applications: recent updates on in vivo study and patents. J Pharm Anal 10:1–12. https://doi.org/10.1016/j.jpha.2019.09.003
15. Kellens E, Bové H, Vandenryt T et al (2018) Micro-patterned molecularly imprinted polymer structures on functionalized diamond-coated substrates for testosterone detection. Biosens Bioelectron 118:58–65. https://doi.org/10.1016/j.bios.2018.07.032
16. Briones M, Casero E, Vázquez L et al (2016) Diamond nanoparticles as a way to improve electron transfer in sol-gel l-lactate biosensing platforms. Anal Chim Acta 908:141–149. https://doi.org/10.1016/j.aca.2015.12.029
17. Briones M, Casero E, Petit-Domínguez MD et al (2015) Diamond nanoparticles based biosensors for efficient glucose and lactate determination. Biosens Bioelectron 68:521–528. https://doi.org/10.1016/j.bios.2015.01.044
18. Saravanan A, Huang BR, Chu JP et al (2019) Interface engineering of ultrananocrystalline diamond/MoS2-ZnO heterostructures and its highly enhanced hydrogen gas sensing properties. Sensors Actuators, B Chem 292:70–79. https://doi.org/10.1016/j.snb.2019.04.108

19. Blanco E, Hristova L, Martínez-Moro R, et al (2020) A 2D tungsten disulphide/diamond nanoparticles hybrid for an electrochemical sensor development towards the simultaneous determination of sunset yellow and quinoline yellow. Sensors Actuators, B Chem 324:.https://doi.org/10.1016/j.snb.2020.128731
20. Rashed MZ, Kopechek JA, Priddy MC et al (2021) Rapid detection of SARS-CoV-2 antibodies using electrochemical impedance-based detector. Biosens Bioelectron 171:112709. https://doi.org/10.1016/j.bios.2020.112709
21. Ibau C, Arshad MKM, Gopinath SCB et al (2020) Immunosensing prostate-specific antigen: Faradaic vs non-Faradaic electrochemical impedance spectroscopy analysis on interdigitated microelectrode device. Int J Biol Macromol 162:1924–1936. https://doi.org/10.1016/j.ijbiomac.2020.08.125
22. Taniselass S, Arshad MKM, Gopinath SCB, Ramli MM (2020) Self-assembled reduced graphene oxide nanoflakes assisted by post-sonication boosted electrical performance in gold interdigitated microelectrodes. J Colloid Interface Sci 577:345–354. https://doi.org/10.1016/j.jcis.2020.05.070
23. Ruwoldt J, Øye G (2020) Effect of low-molecular-weight alcohols on emulsion stabilization with lignosulfonates. ACS Omega 5:30168–30175. https://doi.org/10.1021/acsomega.0c04650
24. Zhang L, Luo Y, Wijayapala R, Walters KB (2017) Alcohol stabilization of low water content pyrolysis oil during high temperature treatment. Energy Fuels 31:13666–13674. https://doi.org/10.1021/acs.energyfuels.7b02276
25. Subramani IG, Perumal V, Gopinath SCB et al (2021) 1,1'-Carbonyldiimidazole-copper nanoflower enhanced collapsible laser scribed graphene engraved microgap capacitive aptasensor for the detection of milk allergen. Sci Rep 11:1–12. https://doi.org/10.1038/s41598-021-00057-4
26. Zhang J, Lakshmipriya T, Gopinath SCB (2020) Electroanalysis on an interdigitated electrode for high-affinity cardiac troponin i biomarker detection by aptamer-gold conjugates. ACS Omega 5:25899–25905. https://doi.org/10.1021/acsomega.0c03260
27. Ramanathan S, Gopinath SCB, Arshad MKM et al (2019) Aluminosilicate nanocomposite on genosensor: a prospective voltammetry platform for epidermal growth factor receptor mutant analysis in non-small cell lung cancer. Sci Rep 9:1–11. https://doi.org/10.1038/s41598-019-53573-9
28. Ramanathan S, Gopinath SCB, Md Arshad MK et al (2019) Assorted micro-scale interdigitated aluminium electrode fabrication for insensitive electrolyte evaluation: zeolite nanoparticle-mediated micro- to nano-scaled electrodes. Appl Phys A 125:548. https://doi.org/10.1007/s00339-019-2833-0
29. Letchumanan I, Md Arshad MK, Balakrishnan SR, Gopinath SCB (2019) Gold-nanorod enhances dielectric voltammetry detection of c-reactive protein: a predictive strategy for cardiac failure. Biosens Bioelectron 130:40–47. https://doi.org/10.1016/j.bios.2019.01.042
30. Ramanathan S, Jusoh M, Sabapathy T, et al (2020) Elastomeric polydimethylsiloxane polymer on conductive interdigitated electrode for analyzing skin hydration dynamics. Appl Phys A Mater Sci Process 126:.https://doi.org/10.1007/s00339-020-03933-4
31. Zheng S, Zhang H, Lakshmipriya T, et al (2019) Gold nanorod integrated electrochemical sensing for hyperglycaemia on interdigitated electrode. Biomed Res Int 2019:.https://doi.org/10.1155/2019/9726967
32. Khan NZ, Chen LY, Lindenbauer A et al (2021) Label-free detection and characterization of heparin-induced thrombocytopenia (HIT)-like antibodies. ACS Omega 6:25926–25939. https://doi.org/10.1021/acsomega.1c02496
33. Zamfir LG, Puiu M, Bala C (2020) Advances in electrochemical impedance spectroscopy detection of endocrine disruptors. Sensors (Switzerland) 20:1–21. https://doi.org/10.3390/s20226443
34. Ramanathan S, Gopinath SCB, Ismail ZH et al (2022) Aptasensing nucleocapsid protein on nanodiamond assembled gold interdigitated electrodes for impedimetric SARS-CoV-2 infectious disease assessment. Biosens Bioelectron 197:113735. https://doi.org/10.1016/j.bios.2021.113735
35. Puthongkham P, Venton BJ (2019) Nanodiamond coating improves the sensitivity and antifouling properties of carbon fiber microelectrodes. ACS Sensors 4:2403–2411. https://doi.org/10.1021/acssensors.9b00994
36. Popov V (2021) Several aspects of application of nanodiamonds as reinforcements for metal matrix composites. Appl Sci 11:.https://doi.org/10.3390/app11104695
37. Wu Y, Weil T (2017) Nanodiamonds for biological applications. Phys Sci Rev 2:1–17. https://doi.org/10.1515/psr-2016-0104
38. Islam MN, Channon RB (2019) Electrochemical sensors. Elsevier Ltd.
39. Rezaei Niya SM, Hoorfar M (2013) Study of proton exchange membrane fuel cells using electrochemical impedance spectroscopy technique - a review. J Power Sources 240:281–293. https://doi.org/10.1016/j.jpowsour.2013.04.011
40. Cruz-Manzo S, Chen R (2013) A generic electrical circuit for performance analysis of the fuel cell cathode catalyst layer through electrochemical impedance spectroscopy. J Electroanal Chem 694:45–55. https://doi.org/10.1016/j.jelechem.2013.01.037
41. Chicco D, Warrens MJ, Jurman G (2021) The coefficient of determination R-squared is more informative than SMAPE, MAE, MAPE, MSE and RMSE in regression analysis evaluation. PeerJ Comput Sci 7:1–24. https://doi.org/10.7717/PEERJ-CS.623
42. Mohanty S, Codell R (2002) Sensitivity analysis methods for identifying influential parameters in a problem with a large number of random variables. Manag Inf Syst 363–374.https://doi.org/10.2495/RISK020361
43. Taleuzzaman M (2018) Limit of blank (LOB), limit of detection (LOD), and limit of quantification (LOQ). Org Med Chem IJ 7:555722. https://doi.org/10.19080/OMCIJ.2018.07.555722
44. Sidhu RK, Cavallaro ND, Pola CC et al (2020) Planar interdigitated aptasensor for flow-through detection of listeria spp. in hydroponic lettuce growth media. Sensors 20:1–20. https://doi.org/10.3390/s20205773
45. Bezerra G, Córdula C, Campos D et al (2019) Electrochemical aptasensor for the detection of HER2 in human serum to assist in the diagnosis of early stage breast cancer. Anal Bioanal Chem 411:6667–6676. https://doi.org/10.1007/s00216-019-02040-5
46. Hideshima S, Wustoni S, Kobayashi M et al (2018) Effect of human serum on the electrical detection of amyloid-β fibrils in biological environments using azo-dye immobilized field effect transistor (FET) biosensor. Sens Bio-Sensing Res 17:25–29. https://doi.org/10.1016/j.sbsr.2018.01.003
47. Purohit B, Vernekar PR, Shetti NP, Chandra P (2020) Biosensor nanoengineering: design, operation, and implementation for biomolecular analysis. Sensors Int 1:100040. https://doi.org/10.1016/j.sintl.2020.100040
48. Kongsuphol P, Ng HH, Pursey JP et al (2014) EIS-based biosensor for ultra-sensitive detection of TNF-α from non-diluted human serum. Biosens Bioelectron 61:274–279. https://doi.org/10.1016/j.bios.2014.05.017
49. Wang X, Zhu Y, Olsen TR et al (2018) A graphene aptasensor for biomarker detection in human serum. Electrochim Acta 290:356–363. https://doi.org/10.1016/j.electacta.2018.08.062
50. Lin CL, Lin CH, Chang HC, Su MC (2015) Protein attachment on nanodiamonds. J Phys Chem A 119:7704–7711. https://doi.org/10.1021/acs.jpca.5b01031
51. Balek L, Buchtova M, Kunova Bosakova M et al (2018) Nanodiamonds as "artificial proteins": regulation of a cell signalling system using low nanomolar solutions of inorganic nanocrystals.

Biomaterials 176:106–121. https://doi.org/10.1016/j.biomaterials.2018.05.030
52. Yakoh A, Pimpitak U, Rengpipat S et al (2021) Paper-based electrochemical biosensor for diagnosing COVID-19: detection of SARS-CoV-2 antibodies and antigen. Biosens Bioelectron 176:112912. https://doi.org/10.1016/j.bios.2020.112912
53. Seo G, Lee G, Kim MJ et al (2020) Rapid detection of COVID-19 causative virus (SARS-CoV-2) in human nasopharyngeal swab specimens using field-effect transistor-based biosensor. ACS Nano 14:5135–5142. https://doi.org/10.1021/acsnano.0c02823
54. Karakuş E, Erdemir E, Demirbilek N, Liv L (2021) Colorimetric and electrochemical detection of SARS-CoV-2 spike antigen with a gold nanoparticle-based biosensor. Anal Chim Acta 1182:338939. https://doi.org/10.1016/j.aca.2021.338939
55. Aydın EB, Aydın M, Sezgintürk MK (2021) Highly selective and sensitive sandwich immunosensor platform modified with MUA-capped GNPs for detection of spike receptor binding domain protein: a precious marker of COVID 19 infection. Sensors Actuators, B Chem 345:130355. https://doi.org/10.1016/j.snb.2021.130355
56. Sender R, Bar-On YM, Gleizer S, Bernshtein B et al (2021) The total number and mass of SARS-CoV-2 virions. PNAS 118:e2024815118. https://doi.org/10.1073/pnas.2024815118